Experimental and Numerical Comparison of Weakly Unstable Detonation using Planar Laser-Induced Fluorescence of Nitric Oxide Imaging

Vigneshwaran Sankar[1,2], Karl P. Chatelain[1,2], Josué Melguizo-Gavilanes[3], Samir B. Rojas Chavez[1,2], Mhedine Alicherif[1,2], Deanna A. Lacoste[1,2]

[1]Mechanical Engineering Program, Physical Science and Engineering Division, King Abdullah University of Science and Technology (KAUST), Thuwal, 23955-6900, Saudi Arabia

[2]Clean Combustion Research Center (CCRC), King Abdullah University of Science and Technology

[3]Institut Pprime, UPR 3346, CNRS, ENSMA, University of Poitiers, Futuroscope-Chasseneuil, France

1 Introduction

Detonations are intense supersonic reactions where the combustion wave propagates at the $\mathcal{O}$(km/s) relative to the unburned fresh gas, accompanied by a pressure rise of $20 - 50$ bar across the wavefront. These reactions are characterized by their high pressure, temperature, and energy release, thus making them of interest for various applications such as propulsion, energy generation, or industrial safety purposes (e.g., nuclear power plant or coal mines). However, due to their complex, multi-dimensional, and unstable nature, detonations are challenging to characterize and predict experimentally and numerically. Commonly used experimental techniques to visualize and/or characterize the detonation structure are smoke foils, non-intrusive techniques such as Schlieren, chemiluminescence, or planar laser-induced fluorescence (PLIF) [1, 2]. Among all these techniques, only a limited number of them can provide quantitative measurements such as the cell size [3], the induction zone length [4], or the temperature profiles [5]. Although it is not possible to extract quantitative quantities (i.e., reaction zone and induction zone lengths) from OH-PLIF only, due to the intense laser absorption at the front [4, 6] and the absence of OH in the induction zone near the shock, structure of the reaction front can be obtained [6, 7]. Rojas Chavez et al. [1, 4] proposed a proof-of-concept to measure the induction zone lengths (Δ_i), within an acceptable level of accuracy (near 2%), using the NO-LIF technique for NO seeded hydrogen detonations mixtures at low pressure. These NO-LIF measurements were recently extended to 2D in [8]. Such visualizations and quantitative measurements can be employed to verify and validate the numerical solver for detonation applications.

In the present study, we made an attempt to evaluate the capabilities of our in-house OpenFOAM-based detonation solver in predicting the experimentally observed (NO-PLIF) features of hydrogen-oxygen detonation diluted with argon at low pressure. Our in-house spectroscopic code [9], called KAT-LIF, is employed to post-process the NO fields and simulate the numerical NO-PLIF image from the simulation. This paper focuses on a qualitative comparison between the numerical and experimental

Correspondence to: vigneshwaran.sankar@kaust.edu.sa

NO-PLIF images at one instant of the wave propagation, for which experimental NO-PLIF images are available. Further quantitative comparisons of induction zone lengths during one cell cycle will be addressed in our future study.

2 Numerical Methodology

Numerical simulations were performed using an OpenFOAM® (OF-v2012) based hybrid solver developed to simulate high-speed reacting flows by incorporating detailed chemistry. This in-house solver is the compilation of native solvers viz., rhoCentralFoam, reactingFoam, and pimpleFoam developed based on [10]. Note that the solver's capability in predicting the global dynamics of detonation transmission in a curved chamber has been tested and validated against experiments in a different OF distribution (v4.1) [11] by conducting laboratory frame of reference simulations. In addition to the non-regression testing, this newer version of the code enables to compute detonation simulation in the shock-attached frame of reference (SFR) to save computational resources. The two-dimensional numerical simulations were performed on a rectangular geometry for a weakly unstable mixture ($2H_2$-O_2-3.76Ar) at 20 kPa and 295 K. The chemistry was modeled with 9 species and 17 reactions from the reduced mechanism of Mével [6]. Although the solver includes the diffusive fluxes in the governing equations, we set viscosity and thermal conductivity to zero for the present study, thus arriving at the reactive Euler equations as shown below.

2.1 Numerical Methods

The solver uses the explicit Kurganov-Tadmor's scheme to preserve the monotonicity across the hydrodynamic discontinuities by retaining a maximum acoustic Courant number of 0.1 for the simulations in the shock-attached frame of reference. Fourth order Rosenbrock ODE (Ordinary Differential Equation) solver is employed to integrate the chemical source terms. The Second-order Crank-Nicholson scheme is used to discretize the time derivatives with adaptive time stepping based on the maximum allowable acoustic Courant number.

2.2 Computational Domain, Initial & Boundary Conditions

The two-dimensional numerical simulation is performed on a rectangular domain of length, $L_x = 15.5\,\text{mm}$, and height, $L_y = 22.5\,\text{mm}$ for a weakly unstable mixture, $2H_2 + O_2 + 3.76\text{Ar}$ at 20 kPa and 295 K in the shock-attached frame of reference. We chose a uniform spatial grid resolution with 24 points per induction zone length ($\Delta_i \approx 240\,\mu$m). This grid system is chosen based on a systematic grid convergence study performed on three grids viz, 16, 24, and 32 points per Δ_i. Of the three grid system, 24 and 32 points per Δ_i show similar smoke foil structure after convergence, indicating that the solution is independent of the grid resolution when at least 24 points per Δ_i are chosen. The solution convergence for all the simulations is decided by ensuring no changes in the cell structure evolution (in terms of regularity and cell size) in the numerical soot foils and the speed of the detonation wave front. Figure 1a illustrates the temperature contour field used as the initial condition, where the fresh gas mixture enters the domain from the left end side at the CJ velocity, $D_{\text{CJ}} = 1804.25$ m/s at 20 kPa and 295 K (obtained from ZNDkin). The post-shock conditions are initialized with a ZND solution, as presented in Figure 1b. Circular hotspots are used to perturb the planar shock and generate a multi-dimensional detonation structure ($p_{\text{ign}} = 50p_0$ and $T_{\text{ign}} = 10T_0$). We use `fixedValue` boundary for all the variables at the inlet, `zeroGradient` boundary condition at the outlets, and `slip` conditions at the top and bottom walls.

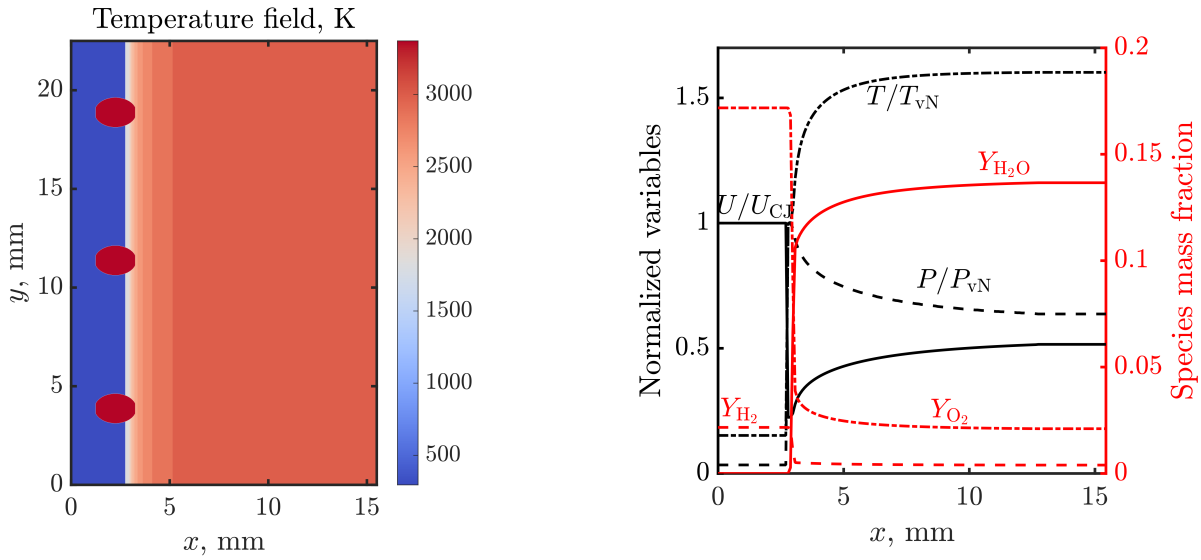

Figure 1: (a) Temperature (K) contour at t = 0 s for the 2D SFR simulation on a 15.5×22.5 mm^2 domain. (b) ZND profiles used for initialization at $t = 0$ s.

2.3 Experimental - Numerical Comparison Procedure

In the present study, the numerical simulation results are compared with the experimental NO-PLIF images obtained from [12] by following the same procedure as in [13] on OH-PLIF. Thus, the NO field, obtained from the numerical simulation, is post-processed by our in-house spectroscopic code, KAT-LIF, to obtain a synthetic (i.e., numerical) NO-PLIF image. Details on KAT-LIF validation and usage can be found in the literature [1,9]. The same experimental setup, optical arrangement, and experimental procedure as [4, 9, 12], was employed to obtain the NO-PLIF images.

3 Results and Discussion

Although the reaction mechanism does not include NO as a species, the numerical NO number density (n_{NO}) is obtained from the other mole fractions by considering a constant concentration of NO ($X_{NO} = 2000$ ppm) within the experimental field of view. Note that the 2000 ppm of NO addition has a negligible effect on the detonation dynamics [4, 14], which enables employing the simulation results from the unseeded mixture to perform the experimental-numerical comparison. In addition, the validity of this constant concentration assumption was confirmed by 1D Zeldovich von Neumann Döring simulations. The results are presented in Fig. 2(a) and evidence a satisfactorily low error (2% up to $40\Delta_i$ from the shock) between the two NO profiles, obtained with the detailed mechanism of Mével [15] and the reconstructed NO profile from the reduced model [6]. As can be seen in Fig. 2(b), X_{NO} between the 2D simulation from OpenFOAM and ZND solution also agrees well near the detonation front (i.e., up to $10\Delta_i$). The discrepancy between the two profiles after $10\Delta_i$ can be attributed to the fact that we are not comparing time-averaged profiles. The region where both the profiles agree well lies within the experimental field-of-view.

Figures 3(a), 3(b), and 3(c) compare the NO number density, the synthetic NO-PLIF, and the experimental NO-PLIF obtained for the considered conditions. The experimental and simulation results show a similar structure of the detonation front (i.e., a Mach stem and an incident shock). The domain size

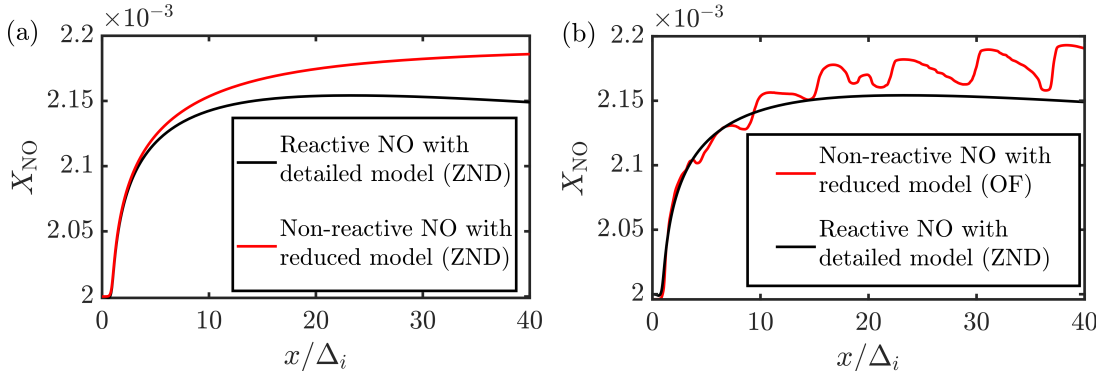

Figure 2: Comparison of NO mole fraction evolution behind the shock front, using ZNDkin, considering the detailed model [15] and the reduced model [6] in (a). Comparison of NO mole fraction between the reduced model, obtained with OpenFOAM simulation, and the detailed model [15], from ZNDkin. The profile from OpenFOAM corresponds to a shock speed near CJ speed.

displayed in Figure 3 are normalized by the corresponding cell size ($\lambda_{exp} \approx 6$ mm and $\lambda_{sim} \approx 4$ mm) to further evidence the similarities. After normalization, the structure of the front looks qualitatively similar between the NO number density, the synthetic NO-PLIF, and the experimental NO-PLIF, while some discrepancies in the intensities can be observed. For more precise comparison, Figure 4 compares the NO number density, the synthetic PLIF intensity, and the experimental PLIF intensity evolution along the lines *A*, *B*, and *C*.

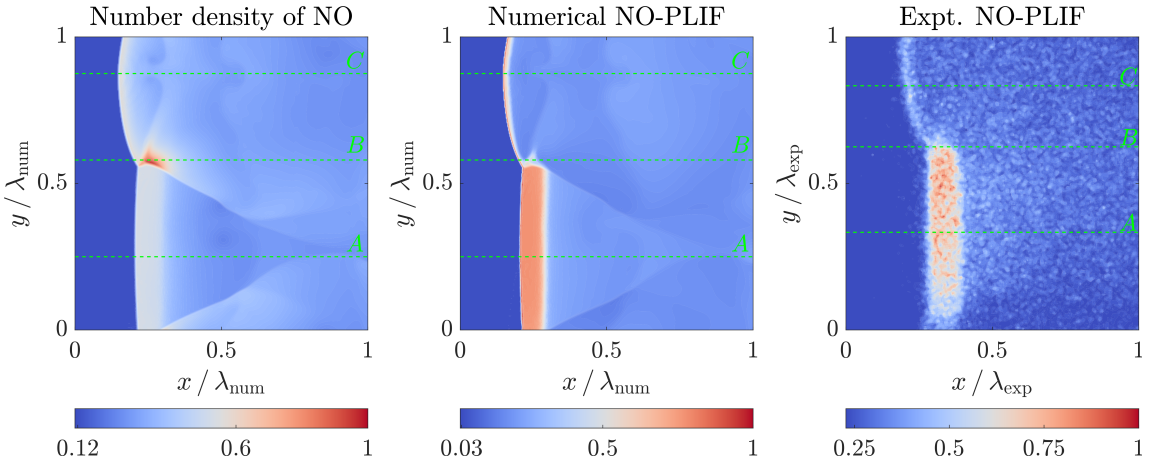

Figure 3: (Left) Normalized non-reactive NO number density from the simulation. (Middle) Numerical NO-PLIF obtained from the KAT-LIF code based on the n_{NO} field on the left. (Right) Experimental NO-PLIF as reported in [12]. The dashed lines (*A*, *B* and *C*) in each figure represents the lines passing through incident shock (IS), triple point (TP) and Mach stem (MS) respectively. The dimensions are normalized by their corresponding mean cell size (λ) in each case.

Qualitatively, the experimental LIF signal is strong in the von Neumann (vN) state and decays rapidly in the reaction zone. This trend is also observed in both the NO number density field and the numerical NO-PLIF images, at the incident shock and the Mach stem (along lines *A* and *C* in Figure 3). This tends to indicate that experimental NO-PLIF images could be directly compared with NO number density fields in these two regions. However, the line passing through the triple point (line *B*), the intensity of the NO number density profile differs significantly from the experimental and KAT-LIF signal. We explain

this discrepancy by the ratio of n_{NO} and quenching rate (a quantity proportional to the LIF signal). We found that quenching rate to be smaller in the region immediately behind the shock in comparison to the n_{NO}. While for $x/\lambda_{num} > 0.28$, the rise in quenching rate is faster in comparison to the rise in n_{NO}, thus causing decay in the LIF signal. The former occurs due to the extreme thermodynamic conditions that influences the quenching rate in NO which explains the disagreement between the n_{NO} and KAT-LIF signal. Also, as previously concluded in [13] for OH-PLIF imaging, the LIF process needs to be modeled in order to compare planar laser-induced fluorescence imaging with numerical simulation results.

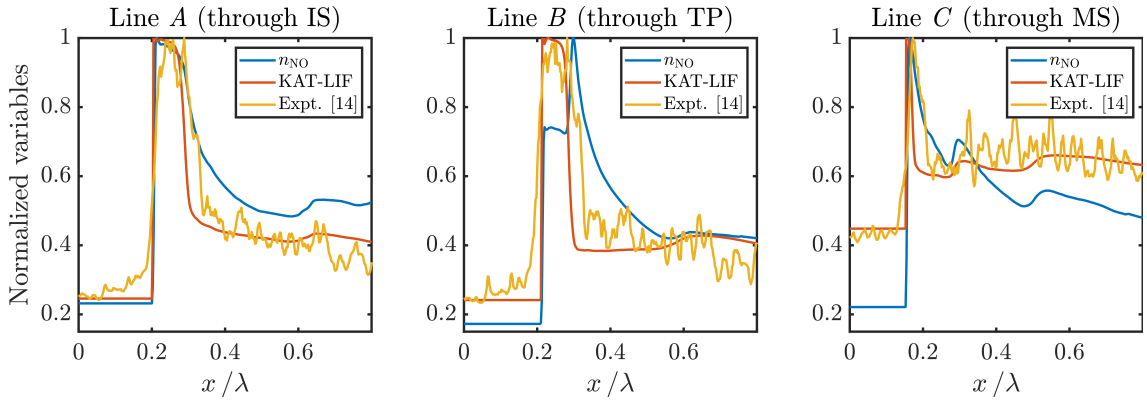

Figure 4: Comparison of normalized n_{NO}, LIF signal from numerical (KAT-LIF) and experimental NO-PLIF along (Left) the line *A* passing through the incident shock (IS), (Middle) the line *B* passing through the triple point, and (Right) the line *C* passing through the Mach stem. To obtain the 1D profile, for the experimental NO-PLIF, the signal is averaged over 280 μm in the y-direction, except for the line *C* where the moving average is performed in the x-direction with an averaging window of 3 pixels (or 42 μm).

4 Concluding Remarks

In the present study, we perform numerical simulations of two-dimensional detonation for a weakly unstable mixture, $2H_2$-O_2-3.76Ar at 20 kPa and 295 K in the shock-attached reference frame using an in-house OpenFOAM-based detonation solver. The convergence of the solution is ensured with: a grid independence study, by ensuring a CJ detonation propagation (near $0.99\times D_{CJ}$), and then monitoring the numerical smoke foils to ensure that their regularity and size do not change significantly. The numerical results are post-processed with KAT-LIF to obtain a synthetic NO-PLIF image. The numerical results are compared and found to be in a qualitative agreement with experimental NO-PLIF images, for most of the locations in the detonation front. Although the structural features and the LIF profile evolution are reproduced by the numerical solutions, the dimensions of the detonation structure ($\lambda_{\text{num}} = 4.44$ mm and $\lambda_{\text{exp}} = 6.7$ mm) deviate by a factor of 1.5. Further quantitative comparisons of induction zone lengths during one cell cycle will be addressed in our future study.

Acknowledgments

This work has been supported by the King Abdullah University of Science and Technology through the baseline fund BAS/1/1396-01-01.

References

[1] S. B. Rojas Chavez, K. P. Chatelain, T. F. Guiberti, R. Mével, and D. A. Lacoste, "Effect of the excitation line on hydroxyl radical imaging by laser induced fluorescence in hydrogen detonations," *Combust. Flame*, vol. 229, p. 111399, 2021.

[2] J. E. Shepherd, "Detonation in gases," *Proc. Comb. Inst.*, vol. 32, no. 1, pp. 83–98, 2009.

[3] R. Strehlow, "Transverse waves in detonations: II. structure and spacing in H_2-O_2, C_2H_2-O_2, C_2H_4-O_2, and CH_4-O_2 systems," *AIAA J.*, vol. 7, pp. 492–496, 1969.

[4] S. B. Rojas Chavez, K. P. Chatelain, and D. A. Lacoste, "Induction zone length measurements by laser-induced fluorescence of nitric oxide in hydrogen-air detonations," *Proc. Comb. Inst.*, 2022.

[5] S. W. Grib, C. A. Fugger, P. S. Hsu, N. Jiang, S. Roy, and S. A. Schumaker, "Two-dimensional temperature in a detonation channel using two-color OH planar laser-induced fluorescence thermometry," *Combust. Flame*, vol. 228, pp. 259–276, 2021.

[6] R. Mével, D. Davidenko, J. Austin, F. Pintgen, and J. Shepherd, "Application of a laser induced fluorescence model to the numerical simulation of detonation waves in hydrogen–oxygen–diluent mixtures," *Int. J. Hydrog. Energy*, vol. 39, no. 11, pp. 6044–6060, 2014.

[7] F. Pintgen, C. Eckett, J. Austin, and J. Shepherd, "Direct observations of reaction zone structure in propagating detonations," *Combust. Flame*, vol. 133, no. 3, pp. 211–229, 2003.

[8] S. B. Rojas Chavez, K. P. Chatelain, and D. A. Lacoste, "Two-dimensional visualization of induction zone in hydrogen detonations," *Combust. Flame*, 2023 (*Submitted*).

[9] K. P. Chatelain, S. B. Rojas Chavez, J. Vargas, and D. A. Lacoste, "Towards laser-induced fluorescence of nitric oxide in detonation," 28th ICDERS, 2022.

[10] M. Kraposhin, A. Bovtrikova, and S. Strijhak, "Adaptation of kurganov-tadmor numerical scheme for applying in combination with the piso method in numerical simulation of flows in a wide range of mach numbers," *Procedia Computer Science*, vol. 66, pp. 43–52, 2015.

[11] J. Melguizo-Gavilanes, V. Rodriguez, P. Vidal, and R. Zitoun, "Dynamics of detonation transmission and propagation in a curved chamber: a numerical and experimental analysis," *Combust. Flame*, vol. 223, pp. 460–473, 2021.

[12] M. Alicherif, K. P. Chatelain, S. B. Rojas Chavez, and D. A. Lacoste, "Induction zone length measurements for regular cell pattern by nitric oxide planar laser-induced fluorescence," 29th ICDERS, 2023 (*Submitted*).

[13] K. P. Chatelain, R. Mével, J. Melguizo-Gavilanes, A. Chinnayya, S. Xu, and D. Lacoste, "Effect of incident laser sheet orientation on the OH-PLIF imaging of detonations," *Shock Waves*, vol. 30, no. 7, pp. 689–702, 2020.

[14] K. P. Chatelain, M. Alicherif, S. B. Rojas Chavez, and D. A. Lacoste, *Nitric oxide sensitization of hydrogen detonations*. National Harbor, Maryland: AIAA Scitech 2023 Forum, 2023, AIAA 2023-1877.

[15] R. Mével, S. Javoy, F. Lafosse, N. Chaumeix, G. Dupré, and C.-E. Paillard, "Hydrogen–nitrous oxide delay times: Shock tube experimental study and kinetic modelling," *Proc. Comb. Inst.*, vol. 32, no. 1, pp. 359–366, 2009.